Izvestiya, Physics of the Solid Earth, Vol. 41, No. 10, 2005, pp. 832–843. Translated from Fizika Zemli, No. 10, 2005, pp. 66–78.

Magnetotelluric Polar Diagrams

M. N. Berdichevsky and R. F. Logunovich

Moscow State University, Vorob'evy gory, Moscow, 119992 Russia
Institute of Geoelectromagnetic Research, Schmidt Institute of Physics of the Earth, Russian Academy of Sciences, Troitsk, Moscow oblast, 142092 Russia

Received February 15, 2005

Abstract—Comparative analysis is performed of magnetotelluric polar diagrams that are helpful for the recognition of geoelectric structures at the stage of qualitative interpretation of magnetotelluric soundings. The following types of polar diagrams are considered: (i) diagrams of the impedance tensor, (ii) diagrams of the *H* and *E* polarized impedances, and (iii) diagrams of the phase tensor. The properties of the diagrams are studied and it is shown that shallow structures of a higher resistivity are identified most reliably with the use of *E* polarized impedance diagrams, whereas phase diagrams of the impedance tensor and diagrams of the phase tensor provide the most reliable constraints on deep (lithospheric) conductive structures. Polar diagrams are free from structural limitations inherent in the standard methods of the separation of local and regional effects. It is important to note that diagrams of the impedance tensor and *E* and *H* polarized impedance diagrams are also free from frequency limitations. Evidently, combined application of polar diagrams significantly widens the possibilities for the separate identification of shallow and deep geoelectric structures.

1. INTRODUCTION

The success of interpretation of magnetotelluric sounding data is largely dependent on the preliminary qualitative analysis intended to construct an interpretation model [Berdichevsky and Dmitriev, 2004]. Geological and geophysical a priori information on the region studied and analysis of measured values of the impedance tensor allow one to perform geoelectric regionalization, localize and identify structures, and determine their dimensions and orientation. Polar diagrams displaying their of magnetotelluric response functions on the structural orientation play an important role at this stage. Modern magnetotellurics provides three types of polar diagrams: (i) diagrams of the impedance tensor, (ii) diagrams of *H* and *E* polarized impedances, and (iii) diagrams of the phase tensor. The goal of our study is a combined analysis of these graphic representations and a comparative analysis of their informativeness.

2. DIAGRAMS OF THE IMPEDANCE TENSOR

This type of polar diagrams was proposed and developed in [Berdichevsky, 1968; Nguen Than Van, 1991; Berdichevsky *et al.*, 1993]. Polar diagrams of the impedance tensor are constructed without structural and frequency limitations.

As is known, the impedance tensor [**Z**] has a square matrix with the diagonal components Z_{xx} and Z_{yy} and the off-diagonal components Z_{xy} and Z_{yx}:

$$[\mathbf{Z}] = \begin{bmatrix} Z_{xx} & Z_{xy} \\ Z_{yx} & Z_{yy} \end{bmatrix}. \qquad (1)$$

The components of the tensor [**Z**] provide information on vertical and horizontal variations in the Earth's electrical conductivity. The main constraints on vertical variations in the conductivity are gained from the off-diagonal components Z_{xy} and Z_{yx}. The diagonal components Z_{xx}, Z_{yy} characterize the geoelectric asymmetry of the medium.

If the *x* and *y* axes are rotated clockwise through an angle α, the components of the tensor [**Z**] change by the law

$$[\mathbf{Z}(\alpha)] = [\mathbf{R}(\alpha)][\mathbf{Z}][\mathbf{R}(\alpha)]^{-1}, \qquad (2)$$

where

$$[\mathbf{R}(\alpha)] = \begin{bmatrix} \cos\alpha & \sin\alpha \\ -\sin\alpha & \cos\alpha \end{bmatrix},$$

$$[\mathbf{R}(\alpha)]^{-1} = \begin{bmatrix} \cos\alpha & -\sin\alpha \\ \sin\alpha & \cos\alpha \end{bmatrix}.$$

Thus, we have

$$|Z_{xx}(\alpha)| = |Z_2 + Z_3\sin 2\alpha + Z_4\cos 2\alpha|,$$
$$|Z_{xy}(\alpha)| = |Z_1 + Z_3\cos 2\alpha - Z_4\sin 2\alpha|, \qquad (3)$$
$$|\arg Z_{xy}(\alpha)| = \left|\arctan\frac{\mathrm{Im}(Z_1 + Z_3\cos 2\alpha - Z_4\sin 2\alpha)}{\mathrm{Re}(Z_1 + Z_3\cos 2\alpha - Z_4\sin 2\alpha)}\right|,$$

where

$$Z_1 = \frac{Z_{xy} - Z_{yx}}{2}, \quad Z_2 = \frac{Z_{xx} + Z_{yy}}{2},$$
$$Z_3 = \frac{Z_{xy} + Z_{yx}}{2}, \quad Z_4 = \frac{Z_{xx} - Z_{yy}}{2}.$$

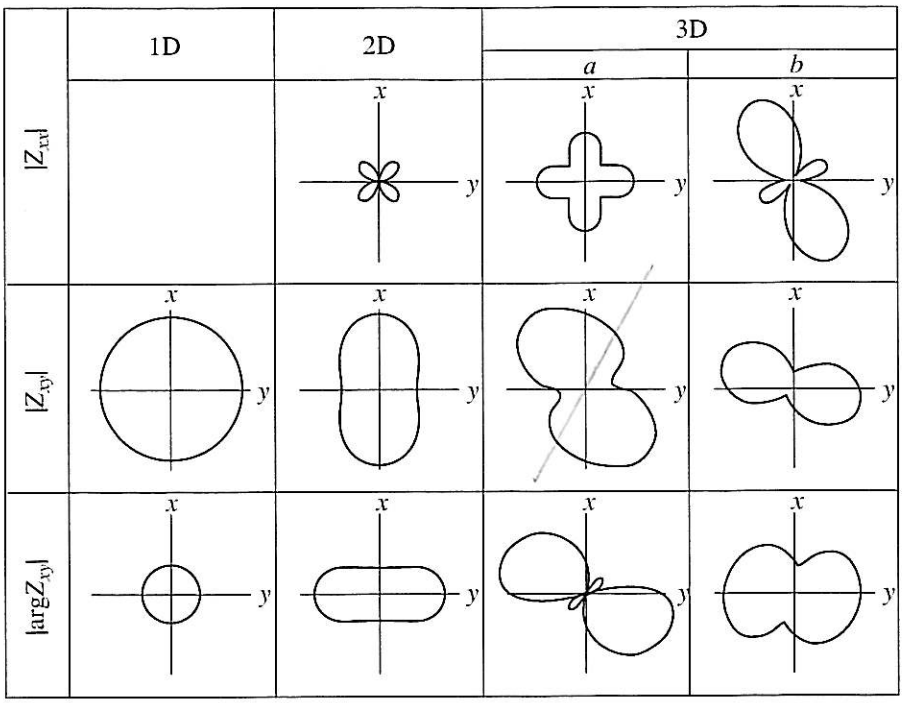

Fig. 1. Polar diagrams $|Z_{xx}|$, $|Z_{xy}|$, and $|\arg Z_{xy}|$ of the impedance tensor [**Z**].

$$\text{1D: } [\mathbf{Z}] = \begin{bmatrix} 0 & 4-2i \\ -4+2i & 0 \end{bmatrix}, \quad skew_S = 0, \quad skew_B = 0;$$

$$\text{2D: } [\mathbf{Z}] = \begin{bmatrix} 0 & 4-2i \\ -1+2i & 0 \end{bmatrix}, \quad skew_S = 0, \quad skew_B = 0;$$

$$\text{3Da: } [\mathbf{Z}] = \begin{bmatrix} -0.5-3i & 4-2i \\ -1+2i & 0.5+3i \end{bmatrix}, \quad skew_S = 0, \quad skew_B = 0.47;$$

$$\text{3Db: } [\mathbf{Z}] = \begin{bmatrix} -0.2+0.2i & -1+3i \\ 0.7-0.5i & 0.5-1.4i \end{bmatrix}, \quad skew_S = 0.32, \quad skew_B = 0.19.$$

Let $|Z_{xx}(\alpha)|$, $|Z_{xy}(\alpha)|$, and $|\arg Z_{xy}(\alpha)|$ be plotted on the x axis making the angle α with the original x axis. As α varies from 0 to 2π, the ends of the corresponding vectors describe closed curves that are polar diagrams of the impedance tensor. The values $|Z_{xx}(\alpha)|$ and $|Z_{xy}(\alpha)|$ form amplitude diagrams, and the value $|\arg Z_{xy}(\alpha)|$ forms a phase diagram. As seen from (3), the amplitude and phase diagrams obey the condition of central symmetry relative to the origin of coordinates:

$$|Z_{xx}(\alpha)| = |Z_{xx}(\alpha+\pi)|, \quad |Z_{xy}(\alpha)| = |Z_{xy}(\alpha+\pi)|,$$
$$|\arg Z_{xy}(\alpha)| = |\arg Z_{xy}(\alpha+\pi)|.$$

The maximum and minimum radii of polar diagrams are determined from the conditions

$$\frac{d|Z_{xx}(\alpha)|}{d\alpha} = 0, \quad \frac{d|Z_{xy}(\alpha)|}{d\alpha} = 0, \quad \frac{d|\arg Z_{xy}(\alpha)|}{d\alpha} = 0. \tag{4}$$

Differentiating these relations, we obtain an equation of degree 4 in $\tan\alpha$. Therefore, the interval $0 \le \alpha \le 2\pi$ can contain four maximums and four minimums of $|Z_{xx}(\alpha)|$, $|Z_{xy}(\alpha)|$, and $|\arg Z_{xy}(\alpha)|$. It is evident that the number of petals in amplitude or phase diagrams cannot exceed four.

Examples of polar diagrams of the impedance tensor that are typical of 1-D, 2-D, and 3-D models are presented in Fig. 1. The shape of these polar diagrams is essentially dependent on the dimensionality and orientation of geoelectric structures.

In a 1-D model, the diagram $|Z_{xx}|$ converges to zero and vanishes and the diagrams $|Z_{xy}|$ and $|\arg Z_{xy}|$ are circles of the radii $|Z|$ and $|\arg Z|$, where Z is the Tikhonov–Cagniard 1-D impedance.

Now, we address a 2-D model striking along the x axis:

$$[\mathbf{Z}] = \begin{bmatrix} 0 & Z^{\parallel} \\ -Z^{\perp} & 0 \end{bmatrix}, \quad (5)$$

where $Z^{\parallel}$ and $Z^{\perp}$ are the longitudinal and transverse impedances (the principal values of the impedance tensor). The necessary conditions of a 2-D model are

$$skew_S = \left|\frac{Z_{xx} + Z_{yy}}{Z_{xy} - Z_{yx}}\right| = 0, \quad (6)$$

$$skew_B = \frac{\sqrt{\left|\mathrm{Im}(Z_{xy}\bar{Z}_{yy} + Z_{xx}\bar{Z}_{yx})\right|}}{|Z_{xy} - Z_{yx}|} = 0, \quad (7)$$

where $skew_S$ is the Swift local parameter of asymmetry and $skew_B$ is the Bahr regional parameter of asymmetry (the line above Z means its complex conjugate).

Substituting (5) into (3), we find the equations of 2-D impedance polar diagrams:

$$|Z_{xx}(\alpha)| = \left|(Z^{\parallel} - Z^{\perp})\sin\alpha\cos\alpha\right|,$$

$$|Z_{xy}(\alpha)| = \left|Z^{\parallel}\cos^2\alpha + Z^{\perp}\sin^2\alpha\right|, \quad (8)$$

$$|\arg Z_{xy}(\alpha)| = \left|\arctan\frac{\mathrm{Im}(Z^{\parallel}\cos^2\alpha + Z^{\perp}\sin^2\alpha)}{\mathrm{Re}(Z^{\parallel}\cos^2\alpha + Z^{\perp}\sin^2\alpha)}\right|.$$

The $|Z_{xx}|$ diagram is a symmetric four-petal rose. The bisectors of the angles between its petals are oriented along and across the strike of the model. The $|Z_{xy}|$ and $|\arg Z_{xy}|$ diagrams appear as regular ovals with more or less narrow necks. Their principal diameters are oriented along and across the strike of the model. As can easily be shown, they are equal to $2|Z^{\parallel}|$, $2|Z^{\perp}|$ and $2|\arg Z^{\parallel}|$, $2|\arg Z^{\perp}|$.

Conditions (6) and (7) are also valid in an axisymmetric 3-D model. In this case, the polar diagrams of the 3-D impedance have the same shape as the polar diagrams of the 2-D impedance. The bisectors of the $|Z_{xx}|$ diagrams and the diameters of the $|Z_{xy}|$ and $|\arg Z_{xy}|$ diagrams are oriented in the radial and the tangential directions.

In 3-D asymmetric models, polar diagrams are irregular and can assume peculiar shapes. Quasi-symmetric models with $skew_S = 0$ and $skew_B \neq 0$ should be considered specially (3Da). In this case, the $|Z_{xx}|$ diagram has the shape of a symmetric cross and the $|Z_{xy}|$ and $|\arg Z_{xy}|$ diagrams can degenerate into a beveled oval with a waist or into a figure eight with a "bow." In the general case (3Db), when $skew_S \neq 0$ and $skew_B \neq 0$, the $|Z_{xx}|$ diagram can have the shape of a figure eight with a bow and the $|Z_{xy}|$ and $|\arg Z_{xy}|$ diagrams can be transformed into ovals with waists.

3. POLAR DIAGRAMS OF *H* AND *E* POLARIZED IMPEDANCES

This method is based on the decomposition of the electromagnetic field into conjugate and associate directions [Counil *et al.*, 1986]. In this case, the field is characterized by such quantities as the "induction intensity" and the "current intensity." Yee and Paulson [1987] proposed a simplified interpretation of the polarization dependences of these quantities.

Note that the terminology used in [Counil *et al.*, 1986; Yee and Paulson, 1987] is vulnerable to criticism. The electric current and electromagnetic induction are interconnected via the Ampère, Faraday, and Ohm laws. An electric current produces a magnetic field that in turn induces an electric field generating an electric current. The intensity of electromagnetic induction depends on the intensity of the inducing current, and the intensity of the induced current depends on the intensity of electromagnetic induction. From the physical standpoint, the separation of these two phenomena is scarcely constructive and only complicates their mathematical description. The formulation of the problem is significantly simplified if the construction of polar diagrams characterizing the field polarization dependence of the scalar indicators used involves the formal terminology, reflecting the mathematical meaning of the values to be determined.

Following Yee and Paulson [1987], we introduce a scalar indicator defined as the ratio of the moduli of electric and magnetic fields with a linear polarization of the magnetic field:

$$Z_H(\alpha_H) = \frac{|\mathbf{E}_\tau|}{|\mathbf{H}_\tau|} = \sqrt{\frac{\mathbf{E}_\tau \cdot \mathbf{E}_\tau}{\mathbf{H}_\tau \cdot \mathbf{H}_\tau}}$$

$$= \sqrt{\frac{|Z_{xx}H_x + Z_{xy}H_y|^2 + |Z_{yx}H_x + Z_{yy}H_y|^2}{|H_x|^2 + |H_y|^2}}$$

$$= \sqrt{\frac{|Z_{xx} + Z_{xy}\tan\alpha_H|^2 + |Z_{yx} + Z_{yy}\tan\alpha_H|^2}{1 + \tan^2\alpha_H}} \quad (9)$$

$$= \sqrt{\frac{k_1\tan^2\alpha_H + k_2\tan\alpha_H + k_3}{1 + \tan^2\alpha_H}}$$

$$= \sqrt{k_1\sin^2\alpha_H + k_2\sin\alpha_H\cos\alpha_H + k_3\cos^2\alpha_H},$$

where

$$k_1 = |Z_{xy}|^2 + |Z_{yy}|^2,$$

$$k_2 = 2\mathrm{Re}(Z_{xx}\bar{Z}_{xy} + Z_{yx}\bar{Z}_{yy}), \quad k_3 = |Z_{xx}|^2 + |Z_{yx}|^2.$$

Here, the modulus $|\mathbf{E}_\tau| = |\mathbf{E}_\tau \cdot \mathbf{E}_\tau| = \sqrt{|E_x|^2 + |E_y|^2}$ of the electric field $\mathbf{E}_\tau(E_x, E_y)$ is normalized to the modulus $|\mathbf{H}_\tau| = \sqrt{\mathbf{H}_\tau \cdot \mathbf{H}_\tau} = \sqrt{|H_x|^2 + |H_y|^2}$ of the magnetic field $\mathbf{H}_\tau(H_x, H_y)$ linearly polarized at an angle α_H to the original x axis. The scalar indicator Z_H can be naturally called an *H* polarized impedance. It is a function of the

angle α_H defining the direction of the magnetic field polarization axis.

The condition

$$\frac{dZ_H}{d\alpha_H} = 0$$

determines the directions providing the maximum and minimum of the H polarized impedance:

$$\tan 2\alpha_H = \frac{k_2}{k_3 - k_1}. \quad (10)$$

This equation has two solutions, $\alpha_H^{\max}$ and $\alpha_H^{\min}$, differing by $\pi/2$.

Similar to the H polarized impedance Z_H, we introduce a scalar indicator Z_E determined as the ratio of the moduli of magnetic and electric fields with a linear polarization of the electric field:

$$Z_E(\alpha) = \frac{|\mathbf{E}_\tau|}{|\mathbf{H}_\tau|} = \sqrt{\frac{\mathbf{E}_\tau \cdot \mathbf{E}_\tau}{\mathbf{H}_\tau \cdot \mathbf{H}_\tau}}$$

$$= \sqrt{\frac{|E_x|^2 + |E_y|^2}{|Y_{xx}E_x + Y_{xy}E_y|^2 + |Y_{yx}E_x + Y_{yy}E_y|^2}} \quad (11)$$

$$= \sqrt{\frac{1 + \tan^2\alpha_E}{|Y_{xx} + Y_{xy}\tan\alpha_E|^2 + |Y_{yx} + Y_{yy}\tan\alpha_E|^2}},$$

where Y_{xx}, Y_{xy}, Y_{yx}, Y_{yy} are the components of the admittance tensor,

$$Y_{xx} = \frac{Z_{yy}}{Z_{xx}Z_{yy} - Z_{xy}Z_{yx}}, \quad Y_{xy} = \frac{Z_{xy}}{Z_{xx}Z_{yy} - Z_{xy}Z_{yx}},$$
$$Y_{yx} = -\frac{Z_{yx}}{Z_{xx}Z_{yy} - Z_{xy}Z_{yx}}, \quad Y_{yy} = \frac{Z_{xx}}{Z_{xx}Z_{yy} - Z_{xy}Z_{yx}}. \quad (12)$$

Here, the modulus $|\mathbf{E}_\tau| = \sqrt{\mathbf{E}_\tau \cdot \mathbf{E}_\tau} = \sqrt{|E_x|^2 + |E_y|^2}$ of the electric field $\mathbf{E}_\tau(E_x, E_y)$ linearly polarized at an angle α_E to the original x axis is normalized to the modulus $|\mathbf{H}_\tau| = \sqrt{\mathbf{H}_\tau \cdot \mathbf{H}_\tau} = \sqrt{|H_x|^2 + |H_y|^2}$ of the magnetic field $\mathbf{H}_\tau(H_x, H_y)$. The scalar indicator Z_E is naturally called an E polarized impedance. It is a function of the angle α_E defining the direction of the electric field polarization axis.

Substituting (12) into (11), we find, after simple calculations,

$$Z_E(\alpha_E) = \sqrt{\frac{1 + \tan^2\alpha_E}{l_1\tan^2\alpha_E - l_2\tan\alpha_E + l_3}}$$

$$= \sqrt{\frac{1}{l_1\sin^2\alpha_E - l_2\sin\alpha_E\cos\alpha_E + l_3\cos^2\alpha_E}}, \quad (13)$$

where

$$l_1 = \frac{|Z_{xx}|^2 + |Z_{xy}|^2}{|Z_{xx}Z_{yy} - Z_{xy}Z_{yx}|^2},$$

$$l_2 = \frac{2\mathrm{Re}(Z_{xx}\bar{Z}_{yx} + Z_{yy}\bar{Z}_{xy})}{|Z_{xx}Z_{yy} - Z_{xy}Z_{yx}|^2}, \quad l_3 = \frac{|Z_{yy}|^2 + |Z_{yx}|^2}{|Z_{xx}Z_{yy} - Z_{xy}Z_{yx}|^2}.$$

The condition

$$\frac{dZ_E}{d\alpha_E} = 0$$

determines the directions providing the maximum and minimum of the E polarized impedance:

$$\tan 2\alpha_E = \frac{l_2}{l_1 - l_3}. \quad (14)$$

This equation has two solutions, $\alpha_E^{\max}$ and $\alpha_E^{\min}$, differing by $\pi/2$.

No structural or frequency limitations are involved in the construction of polar diagrams of the H and E polarized impedances.

Let $Z_H(\alpha_H)$ be laid off on the polarization axis of the magnetic field. As the angle α_H varies from 0 to 2π, the end of the corresponding vector describes a closed curve that is the polar diagram of the H polarized impedance. The polar diagram $I_Z(\alpha_H)$ is a regular oval determined by Eq. (9). If the radius $Z_H(\alpha_H)$ is replaced by the radius $1/Z_H(\alpha_H)$, the oval is transformed into an ellipse.

Let $Z_E(\alpha_E)$ be laid off on the polarization axis of the electric field. As the angle α_E varies from 0 to 2π, the end of the corresponding vector describes a closed curve that is the polar diagram of the E polarized impedance. The polar diagram I is an ellipse determined by the equation

$$l_1 Z_E^2 \sin^2\alpha_E - l_2 Z_E^2 \sin\alpha_E\cos\alpha_E + l_3 Z_E^2\cos^2\alpha_E = 1.$$

Following Counil *et al.* [1986], we introduce an angular skew parameter in accordance with (10) and (14):

$$skew_{CLM} = \alpha_E^{\max} - \alpha_H^{\min} = \alpha_H^{\max} - \alpha_E^{\min}$$
$$= \arctan\mathrm{Re}\frac{Z_{xx} + Z_{yy}}{Z_{yx} - Z_{xy}}. \quad (15)$$

This parameter characterizes the mutual orientation of the polar diagrams of the H and E polarized impedances. Here, the angles $\alpha_E^{\max}$, $\alpha_E^{\min}$ and $\alpha_H^{\max}$, $\alpha_H^{\min}$ define the directions of the maximum and minimum diameters of the polar diagrams. Note that $skew_{CLM} = 0$ if $skew_S = 0$; i.e., the diagrams of the H and E polarized impedances are elongated in perpendicular directions.

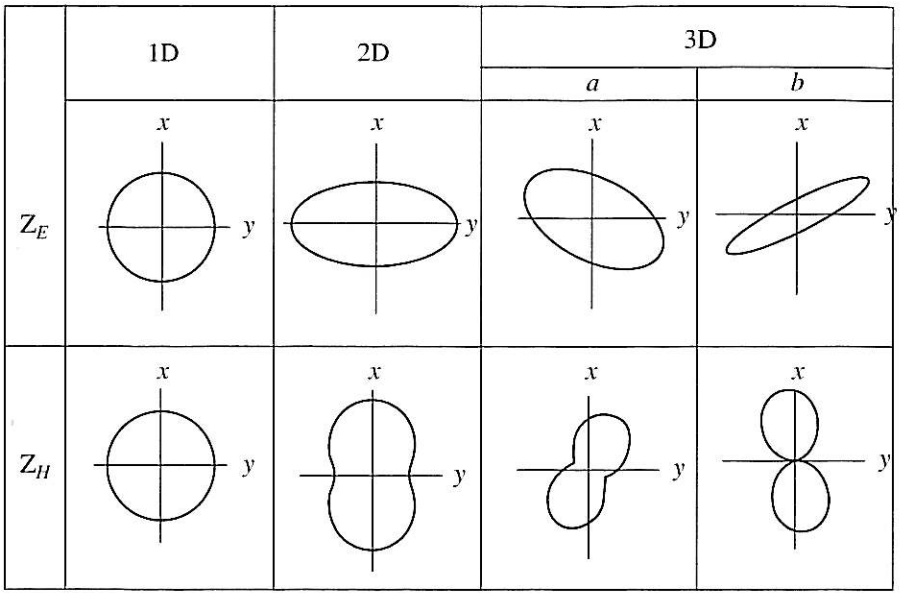

Fig. 2. Polar diagrams of the H polarized (Z_H) and E polarized (Z_E) impedances.

$$\text{1D: } [\mathbf{Z}] = \begin{bmatrix} 0 & 4-2i \\ -4+2i & 0 \end{bmatrix}, \quad skew_S = 0, \quad skew_B = 0;$$

$$\text{2D: } [\mathbf{Z}] = \begin{bmatrix} 0 & 4-2i \\ -1+2i & 0 \end{bmatrix}, \quad skew_S = 0, \quad skew_B = 0;$$

$$\text{3Da: } [\mathbf{Z}] = \begin{bmatrix} -0.5-3i & 4-2i \\ -1+2i & 0.5+3i \end{bmatrix}, \quad skew_S = 0, \quad skew_B = 0.47;$$

$$\text{3Db: } [\mathbf{Z}] = \begin{bmatrix} -0.2+0.2i & -1+3i \\ 0.7-0.5i & 0.5-1.4i \end{bmatrix}, \quad skew_S = 0.32, \quad skew_{CLM} = 20^\circ, \quad skew_B = 0.19.$$

Examples of polar diagrams of the H and E polarized impedances typical of 1-D, 2-D, and 3-D models are presented in Fig. 2.

The Z_H and Z_E diagrams in a 1-D model are circles of the radius $|Z|$, where Z is the Tikhonov–Cagniard 1-D impedance.

Now, we address a 2-D model striking along the x axis. According to (5), we have

$$Z_{xy} = 0, \quad Z_{xy} = Z^{\parallel}, \quad Z_{yx} = -Z^{\perp}, \quad Z_{yy} = 0,$$

where $Z^{\parallel}$ and $Z^{\perp}$ are the longitudinal and transverse impedances. Substituting (5) into (9) and (13), we find

$$Z_H(\alpha_H) = \sqrt{|Z^{\parallel}|^2 \sin^2\alpha_H + |Z^{\perp}|^2 \cos^2\alpha_H},$$
$$Z_E(\alpha_E) = \sqrt{\frac{1}{\dfrac{\sin^2\alpha_E}{|Z^{\perp}|^2} + \dfrac{\cos^2\alpha_E}{|Z^{\parallel}|^2}}}. \qquad (16)$$

The polar diagrams of the H and E polarized impedances have the respective shapes of a regular oval with a waist and an ellipse. Their principal diameters are oriented along and across the strike of the model and are equal to $2|Z^{\parallel}|$ and $2|Z^{\perp}|$, respectively. The Z_H and Z_E diagrams in an axisymmetric 3-D model have similar shapes, with their principal diameters being oriented along the radial and the tangential directions, respectively.

In a quasi-symmetric 3-D model (3Da) with $skew_S = skew_{CLM} = 0$, the diagrams of Z_H and Z_E retain a regular shape and are elongated in perpendicular directions. In an asymmetric 3-D model (3Db) with $skew_{CLM} \neq 0$, a regular shape of the Z_H and Z_E diagrams is preserved but the angle between their elongation directions can deviate significantly from a right angle. This is the only feature of the Z_H and Z_E diagrams that can be used as an indicator distinguishing an asymmetric 3-D medium from a 2-D or an axisymmetric 3-D medium.

4. POLAR DIAGRAMS OF THE PHASE TENSOR

The method of the phase tensor proposed by Caldwell *et al.* [2004] is one of the most interesting novel tools of modern magnetotellurics. This method is effective for eliminating geological noise caused by small

shallow heterogeneities and gaining reliable constraints on deep regional structures of any dimensionality.

We remind the reader of the idea of the phase tensor. In the range of rather low frequencies, the tensor of magnetotelluric impedance [**Z**] distorted by small shallow (2-D or 3-D) heterogeneities can be represented as

$$[\mathbf{Z}] = [\mathbf{e}][\mathbf{Z}^R], \tag{17}$$

where [**e**] is the real matrix of galvanic distortions of the electric field,

$$[\mathbf{e}] = \begin{bmatrix} e_{xx} & e_{xy} \\ e_{yx} & e_{yy} \end{bmatrix},$$

and $[\mathbf{Z}^R]$ is the tensor of the undistorted regional impedance reflecting the structure of deep heterogeneous (2-D or 3-D) zones,

$$[\mathbf{Z}^R] = \begin{bmatrix} Z^R_{xx} & Z^R_{xy} \\ Z^R_{yx} & Z^R_{yy} \end{bmatrix}.$$

Here, the low-frequency magnetic anomaly produced by a shallow local heterogeneity is assumed to be negligibly small and is not considered.

The real phase tensor

$$[\mathbf{\Phi}] = \begin{bmatrix} \Phi_{xx} & \Phi_{xy} \\ \Phi_{yx} & \Phi_{yy} \end{bmatrix}$$

is defined as the product of the inverse real tensor $[\mathrm{Re}\mathbf{Z}]^{-1}$ and the imaginary tensor [Im**Z**]:

$$\begin{aligned}[\mathbf{\Phi}] &= [\mathrm{Re}\mathbf{Z}]^{-1}[\mathrm{Im}\mathbf{Z}] = [\mathrm{Re}\mathbf{Z}^R]^{-1}[\mathbf{e}]^{-1}[\mathbf{e}][\mathrm{Im}\mathbf{Z}^R] \\ &= [\mathrm{Re}\mathbf{Z}^R]^{-1}[\mathrm{Im}\mathbf{Z}^R] = [\mathbf{\Phi}^R].\end{aligned} \tag{18}$$

It is evident that the phase tensor depends on the regional structure alone. Using matrix transformations, we eliminate the effect of shallow local structures (geological noise):

$$\begin{aligned}\Phi_{xx} &= \frac{\mathrm{Re}Z_{yy}\mathrm{Im}Z_{xx} - \mathrm{Re}Z_{xy}\mathrm{Im}Z_{yx}}{\mathrm{Re}Z_{xx}\mathrm{Re}Z_{yy} - \mathrm{Re}Z_{xy}\mathrm{Re}Z_{yx}} \\ &= \frac{\mathrm{Re}Z^R_{yy}\mathrm{Im}Z^R_{xx} - \mathrm{Re}Z^R_{xy}\mathrm{Im}Z^R_{yx}}{\mathrm{Re}Z^R_{xx}\mathrm{Re}Z^R_{yy} - \mathrm{Re}Z^R_{xy}\mathrm{Re}Z^R_{yx}}, \\ \Phi_{xy} &= \frac{\mathrm{Re}Z_{yy}\mathrm{Im}Z_{xy} - \mathrm{Re}Z_{xy}\mathrm{Im}Z_{yy}}{\mathrm{Re}Z_{xx}\mathrm{Re}Z_{yy} - \mathrm{Re}Z_{xy}\mathrm{Re}Z_{yx}} \\ &= \frac{\mathrm{Re}Z^R_{yy}\mathrm{Im}Z^R_{xy} - \mathrm{Re}Z^R_{xy}\mathrm{Im}Z^R_{yy}}{\mathrm{Re}Z^R_{xx}\mathrm{Re}Z^R_{yy} - \mathrm{Re}Z^R_{xy}\mathrm{Re}Z^R_{yx}}, \\ \Phi_{yx} &= \frac{\mathrm{Re}Z_{xx}\mathrm{Im}Z_{yx} - \mathrm{Re}Z_{yx}\mathrm{Im}Z_{xx}}{\mathrm{Re}Z_{xx}\mathrm{Re}Z_{yy} - \mathrm{Re}Z_{xy}\mathrm{Re}Z_{yx}} \\ &= \frac{\mathrm{Re}Z^R_{xx}\mathrm{Im}Z^R_{yx} - \mathrm{Re}Z^R_{yx}\mathrm{Im}Z^R_{xx}}{\mathrm{Re}Z^R_{xx}\mathrm{Re}Z^R_{yy} - \mathrm{Re}Z^R_{xy}\mathrm{Re}Z^R_{yx}}, \\ \Phi_{yy} &= \frac{\mathrm{Re}Z_{xx}\mathrm{Im}Z_{yy} - \mathrm{Re}Z_{yx}\mathrm{Im}Z_{xy}}{\mathrm{Re}Z_{xx}\mathrm{Re}Z_{yy} - \mathrm{Re}Z_{xy}\mathrm{Re}Z_{yx}} \\ &= \frac{\mathrm{Re}Z^R_{xx}\mathrm{Im}Z^R_{yy} - \mathrm{Re}Z^R_{yx}\mathrm{Im}Z^R_{xy}}{\mathrm{Re}Z^R_{xx}\mathrm{Re}Z^R_{yy} - \mathrm{Re}Z^R_{xy}\mathrm{Re}Z^R_{yx}}.\end{aligned} \tag{19}$$

The technique of polar diagrams developed for the impedance tensor [**Z**] can be applied to the phase tensor [**Φ**] without any structural limitations, but its application requires sufficiently low frequencies because, in determining the phase tensor, we neglect magnetic anomalies produced by shallow heterogeneities.

If the axes x and y are rotated clockwise through an angle α, components of the tensor [**Φ**] change by the law

$$[\mathbf{\Phi}(\alpha)] = [\mathbf{R}(\alpha)][\mathbf{\Phi}][\mathbf{R}(\alpha)]^{-1}; \tag{20}$$

hence, we obtain

$$\begin{aligned}\Phi_{xx}(\alpha) &= \Phi_2 + \Phi_3\sin 2\alpha + \Phi_4\cos 2\alpha, \\ \Phi_{xy}(\alpha) &= \Phi_1 + \Phi_3\cos 2\alpha - \Phi_4\sin 2\alpha,\end{aligned} \tag{21}$$

where

$$\Phi_1 = \frac{\Phi_{xy} - \Phi_{yx}}{2}, \quad \Phi_2 = \frac{\Phi_{xx} + \Phi_{yy}}{2},$$
$$\Phi_3 = \frac{\Phi_{xy} + \Phi_{yx}}{2}, \quad \Phi_4 = \frac{\Phi_{xx} - \Phi_{yy}}{2}.$$

Let the values $\varphi_{xx}(\alpha) = |\arctan\Phi_{xx}(\alpha)|$ and $\varphi_{xy}(\alpha) = |\arctan\Phi_{xy}(\alpha)|$ be laid off on the x axis. If α varies from 0 to 2π, the ends of the corresponding vectors describe the closed curves

$$\begin{aligned}\varphi_{xx}(\alpha) &= |\arctan(\Phi_2 + \Phi_3\sin 2\alpha + \Phi_4\cos 2\alpha)|, \\ \varphi_{xy}(\alpha) &= |\arctan(\Phi_1 + \Phi_3\cos 2\alpha - \Phi_4\sin 2\alpha)|;\end{aligned} \tag{22}$$

these curves are the polar diagrams of the phase tensor. Like the diagrams of the impedance tensor [**Z**], the diagrams of the phase tensor [**Φ**] are antisymmetric with respect to any line passing through the origin of coordinates and assume the shape of regular or irregular ovals or can have four petals.

Examples of polar diagrams of the phase tensor typical of 1-D, 2-D, and 3-D models are presented in Fig. 3. Polar diagrams of the phase tensor, as in the case of the impedance tensor, are essentially dependent on the dimensionality and orientation of geoelectric structures.

For a 1-D model, we have

$$\Phi_{xx} = \Phi_{yy} = \tan\arg Z, \quad \Phi_{xy} = \Phi_{yx} = 0,$$

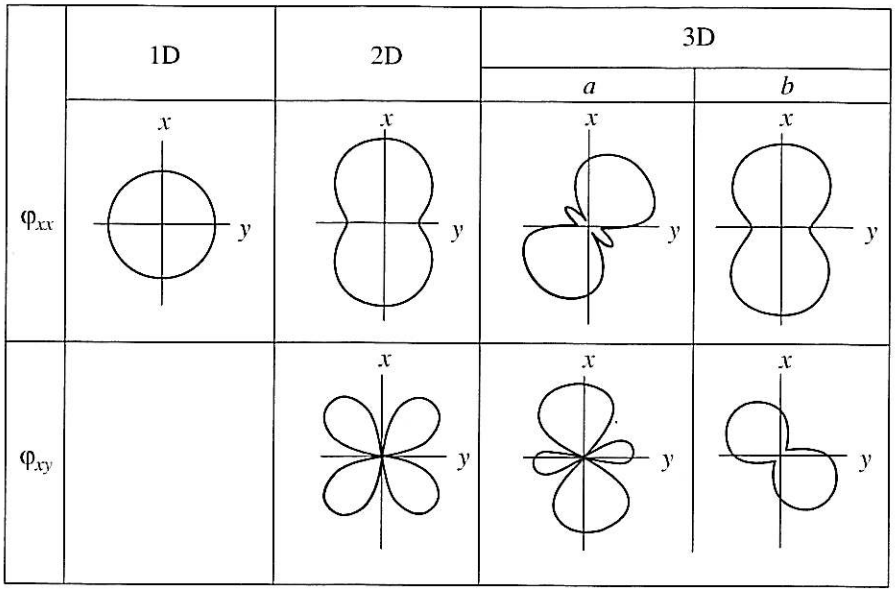

Fig. 3. Polar diagrams φ_{xx} and φ_{xy} of the phase tensor $[\Phi]$.

1D: $[\mathbf{Z}] = \begin{bmatrix} 0 & 4-2i \\ -4+2i & 0 \end{bmatrix}$, $skew_S = 0$, $skew_B = 0$;

2D: $[\mathbf{Z}] = \begin{bmatrix} 0 & 4-2i \\ -1+2i & 0 \end{bmatrix}$, $skew_S = 0$, $skew_B = 0$;

3Da: $[\mathbf{Z}] = \begin{bmatrix} -0.5-3i & 4-2i \\ -1+2i & 0.5+3i \end{bmatrix}$, $skew_S = 0$, $skew_B = 0.47$;

3Db: $[\mathbf{Z}] = \begin{bmatrix} -0.5-3i & 4-2i \\ -1+2i & 0.1-i \end{bmatrix}$, $skew_S = 0.63$, $skew_B = 0.44$.

where Z is the Tikhonov–Cagniard 1-D impedance. In this case, the φ_{xx} diagram is a circle of the radius $|\arg\mathbf{Z}|$ and the φ_{xy} diagram converges to zero and vanishes:

$$\varphi_{xx}(\alpha) = |\arg Z|, \quad \varphi_{xy} = 0. \tag{23}$$

For a 2-D model striking along the x axis, we have

$$\Phi_{xx} = \tan\arg Z^{\perp}, \quad \Phi_{yy} = \tan\arg Z^{\parallel},$$
$$\Phi_{xy} = \Phi_{yx} = 0;$$

hence, we obtain

$$\varphi_{xx}(\alpha) = \left|\arctan\left(\tan\arg Z^{\perp}\cos^2\alpha + \tan\arg Z^{\parallel}\sin^2\alpha\right)\right|,$$
$$\varphi_{xy}(\alpha) = \left|\arctan\left\{\left(\tan\arg Z^{\perp} - \tan\arg Z^{\parallel}\right)\sin\alpha\cos\alpha\right\}\right|, \tag{24}$$

where $Z^{\perp}$ and $Z^{\parallel}$ are the transverse and longitudinal impedances. The φ_{xx} diagram assumes here the shape of a regular oval with a distinct waist. Its principal diameters are oriented in the longitudinal and transverse directions and are equal to the moduli of the doubled phases of the respective impedances. The φ_{xy} diagram has the shape of a symmetric four-petal rose. The bisectors of the angles between the petals are oriented in the longitudinal and transverse directions. The polar diagrams of the phase tensor in an axisymmetric 3-D model have similar shapes.

Asymmetry of a 3-D model leads to polar diagrams of an irregular shape. In the quasi-symmetric case (3Da) with $skew_S = 0$ and $skew_B \neq 0$, the phase tensor diagrams can appear as figure eights with "bows"; in the general case with $skew_S \neq 0$ and $skew_B \neq 0$ (3Db), they assume the shape of a figure eight or an oval with a waist.

5. MAGNETOTELLURIC POLAR DIAGRAMS OF A MODEL CONTAINING SHALLOW AND DEEP STRUCTURES

As an example, we address a three-layer model consisting of a conducting sedimentary cover, a high-resistivity lithosphere, and a well-conducting mantle (Fig. 4a). The sedimentary layer contains a higher resistivity small-scale Γ-shaped inclusion. The lithosphere contains a regional-scale 2-D rectangular prism of a lower resistivity elongated along the x axis. The width of the prism is much larger than the size of the local shallow

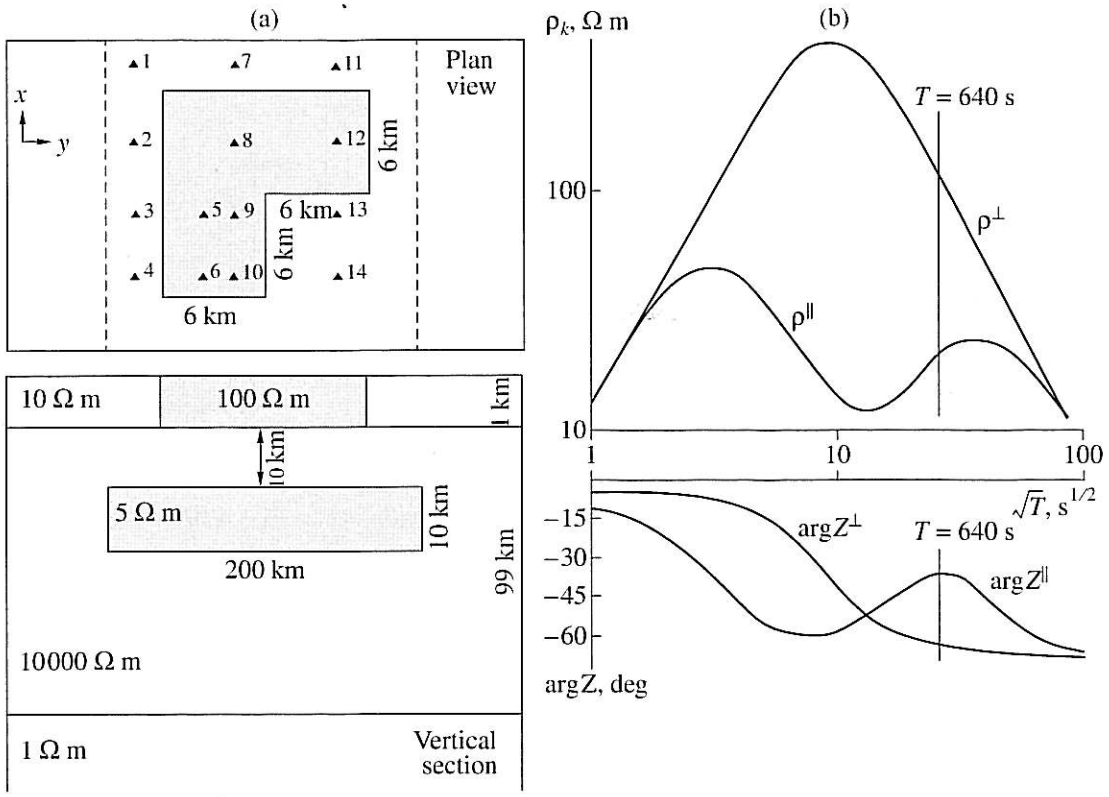

Fig. 4. Model containing a local shallow Γ-shaped inclusion and a deep regional 2-D prism: (a) plan view and vertical section of the model; (b) longitudinal (||) and transverse (⊥) curves of apparent resistivities and impedance phases above the midpoint of the regional prism (in the absence of a shallow inclusion).

inclusion. Evidently, the regional field of the prism can be considered uniform in the area of the inclusion.

The values of the impedance tensor are given at 14 points above and in the vicinity of the inclusion. The problem is solved by means of the hybrid method proposed in [Berdichevsky and Dmitriev, 1976]. This method is based on a local–regional (LR) decomposition of the impedance expressing the tensor [**Z**] through the tensor of regional impedance [$\mathbf{Z}^R$] and the 2 × 2 matrices of electric and magnetic local distortions [**e**] and [**h**]:

$$[\mathbf{Z}] = [\mathbf{e}][\mathbf{Z}^R][\mathbf{h}]^{-1}. \quad (25)$$

Calculations are performed in three stages.

At the first stage, the problem is solved for the 2-D regional prism in the absence of the local shallow inclusion. The tensor of the regional impedance

$$[\mathbf{Z}^R] = \begin{bmatrix} 0 & Z^{\parallel} \\ -Z^{\perp} & 0 \end{bmatrix} \quad (26)$$

is calculated above the midpoint of the prism.

At the second stage, the distortion matrices [**e**] and [**h**] are determined. The shallow Γ-shaped inclusion is placed in the sedimentary cover, and the regional prism is replaced by an infinite horizontally homogeneous layer of the same thickness and resistivity. This 3-D problem is solved in the low frequency approximation of an S thin layer. We obtain the electric distortion matrix

$$[\mathbf{e}] = \begin{bmatrix} e_{xx} & e_{xy} \\ e_{yx} & e_{yy} \end{bmatrix}. \quad (27)$$

The magnetic distortion matrix is calculated from the excess current **J** spreading in the sedimentary cover:

$$\mathbf{J} = S\mathbf{E}_\tau - S_1\mathbf{E}_\tau^R, \quad (28)$$

where $\mathbf{E}_\tau$ is the total electric field, $\mathbf{E}_\tau^R$ is the regional electric field, and S is the conductance of the sediments,

$$S = \begin{cases} S_1 = h_1/\rho_1 & \text{outside the } \Gamma\text{-shaped inclusion} \\ S_\Gamma = h_1/\rho_\Gamma & \text{inside the } \Gamma\text{-shaped inclusion.} \end{cases}$$

The horizontal components of the anomalous magnetic field $\mathbf{H}_\tau^A$ produced by the excess current **J** at the upper and lower boundaries of the cover coincide in value and are opposite in sign. We have at the Earth's surface:

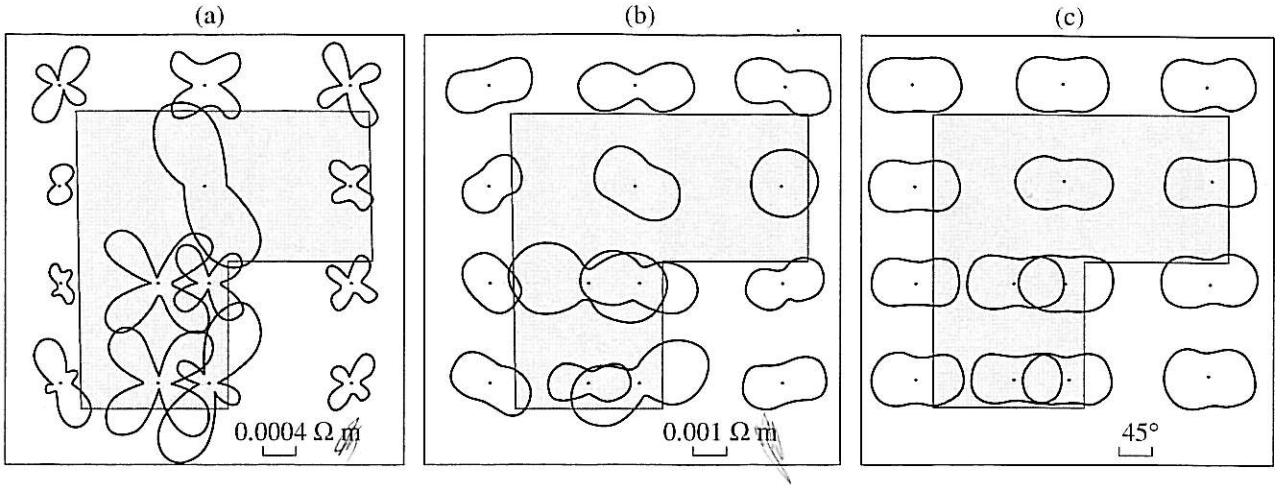

Fig. 5. Polar diagrams of the impedance tensor above the Γ-shaped inclusion: (a) $|Z_{xx}|$; (b) $|Z_{xy}|$; (c) $|\arg Z_{xy}|$.

$$\mathbf{H}_\tau^A = \frac{1}{2}[\mathbf{R}(-\pi/2)]\mathbf{J} = \frac{1}{2}[\mathbf{R}(-\pi/2)](S\mathbf{E}_\tau - S_\Gamma\mathbf{E}_\tau^R) \quad (29)$$
$$= \frac{1}{2}[\mathbf{R}(-\pi/2)](S[\mathbf{e}] - S_\Gamma[\mathbf{I}])\mathbf{E}_\tau^R = [\tilde{\mathbf{h}}]\mathbf{E}_\tau^R,$$

where

$$[\tilde{\mathbf{h}}] = \frac{1}{2}[\mathbf{R}(-\pi/2)](S[\mathbf{e}] - S_\Gamma[\mathbf{I}]),$$

$$[\mathbf{R}(-\pi/2)] = \begin{bmatrix} 0 & -1 \\ 1 & 0 \end{bmatrix}, \quad [\mathbf{I}] = \begin{bmatrix} 1 & 0 \\ 0 & 1 \end{bmatrix}.$$

As a result, we obtain the total magnetic field

$$\mathbf{H}_\tau = [\mathbf{h}]\mathbf{H}_\tau^R, \quad (30)$$

where $\mathbf{H}_\tau^R$ is the regional magnetic field and $[\mathbf{h}]$ is the magnetic distortion matrix,

$$[\mathbf{h}] = [\mathbf{I}] + [\tilde{\mathbf{h}}][\mathbf{Z}^R] = \begin{bmatrix} h_{xx} & h_{xy} \\ h_{yx} & h_{yy} \end{bmatrix}. \quad (31)$$

At the final stage, we substitute (26), (27), and (31) into (25) and synthesize the tensor of the impedance distorted by the local and regional heterogeneities.

Now, we consider the magnetotelluric polar diagrams obtained Γ-shaped from the values of $[\mathbf{Z}]$ synthesized at $T = 640$ s. Figure 4b shows that the effect of the deep conducting prism is well resolved at this period.

As noted above, neither structural nor frequency limitations are imposed on polar diagrams of the tensors of impedance and H and E polarized impedances, whereas polar diagrams of the phase tensor are constructed under the assumption that shallow magnetic anomalies are negligible.

Polar diagrams of the impedance tensor are shown in Fig. 5. The amplitude diagrams of $|Z_{xx}|$ and $|Z_{xy}|$ indicate a strong effect of the local shallow inclusion. The behavior of the $|Z_{xx}|$ diagrams is difficult to interpret: no regular patterns are observable in variations in their shape and orientation, and only the inclusion can be approximately localized. On the other hand, the $|Z_{xy}|$ diagrams are typically regular ovals with a variously narrow waist. The smooth variations in their orientation indicate that the current flows around the higher resistivity Γ-shaped inclusion. Inspecting these diagrams, we can, to an extent, determine the geometry of the inclusion and estimate its resistivity. The phase diagrams $|\arg Z_{xy}|$ are most interesting: they are free from the distorting effect of the shallow inclusion and have the shape of nearly identical ovals with a noticeable waist that are elongated across the strike of the regional prism. The direction of the minimum diameter defines the strike azimuth of the prism, and the values of the maximum and minimum half-diameters yield the phase moduli of the transverse and longitudinal regional impedances $|\arg Z^{\parallel}|$ and $|\arg Z^{\perp}|$. The uncertainties of these determinations do not exceed 5°.

Polar diagrams of the H and E polarized impedances are presented in Fig. 6. The diagrams clearly show the strong distorting effect of the shallow higher resistivity Γ-shaped inclusion. The Z_E diagrams are most informative: their orientation changes rather sharply at many points and yields a clear picture of a flow around a high-resistivity asymmetric body. The 3-D nature of the shallow inclusion is additionally emphasized by the fact that the angle between the elongation directions of the Z_H and Z_E diagrams shown at several points obviously differs from $\pi/2$.

Polar diagrams of the phase tensor are shown in Fig. 7. At most points, the φ_{xx} diagrams have the shape of nearly identical regular ovals with a noticeable waist that are elongated in a direction close to the strike of the regional conducting prism. Being analogues of the

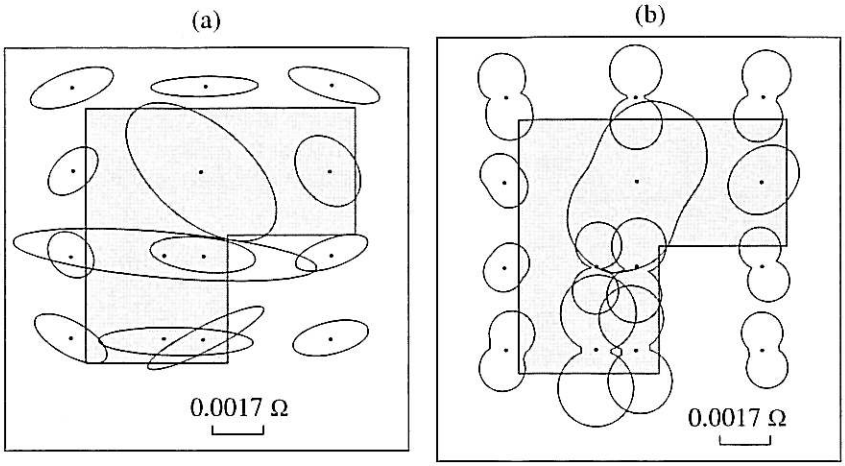

Fig. 6. Polar diagrams of the H and E polarized impedances above the Γ-shaped inclusion: (a) Z_H; (b) Z_E.

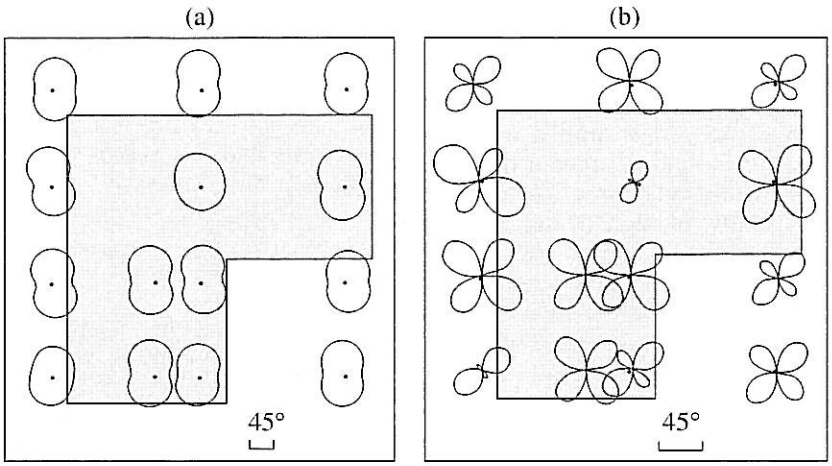

Fig. 7. Polar diagrams of the phase tensor above the Γ-shaped inclusion: (a) φ_{xx}; (b) φ_{xy}.

phase diagrams of the impedance tensor, they are similar to them in shape but are oriented at a right angle to them. The direction of the maximum diameters of the φ_{xx} diagrams defines the strike azimuth of the prism, and the values of the minimum and maximum half-diameters yield estimates for the phase moduli of the transverse and longitudinal impedances $|\arg Z^{\parallel}|$ and $|\arg Z^{\perp}|$. The uncertainties of these determinations do not exceed 5° at most points but reach 10°–12° at three points. The φ_{xy} diagrams at nearly all points have the shape of roses with four more or less identical petals (the evidence for a 2-D regional structure) and the bisectors between the petals are directed along and across the strike of the regional prism. A deviation from this pattern is observed at two points, apparently, because shallow anomalies of the magnetic field were not allowed for there.

6. CONCLUSION

The above analysis has clearly demonstrated the following properties of magnetotelluric polar diagrams. Amplitude diagrams of the impedance tensor $|Z_{xx}|$ and $|Z_{xy}|$ and diagrams of the H and E polarized impedances Z_H and Z_E reflect the influence of local shallow structures in a wide range of frequencies. At relatively low frequencies, phase diagrams of the impedance tensor $|\arg Z_{xy}|$ and diagrams of the phase tensor φ_{xx} and φ_{xy} characterize regional deep structures, with the distorting influence of local shallow structures being weak. Therefore, combined analysis of polar diagrams of different magnetotelluric response functions can be successfully used for discrimination between local and regional effects. In the case of a higher resistivity shallow inclusion, this analysis is most effective with the use of E polarized impedance diagrams, clearly characterizing the structure of the near-surface medium, and

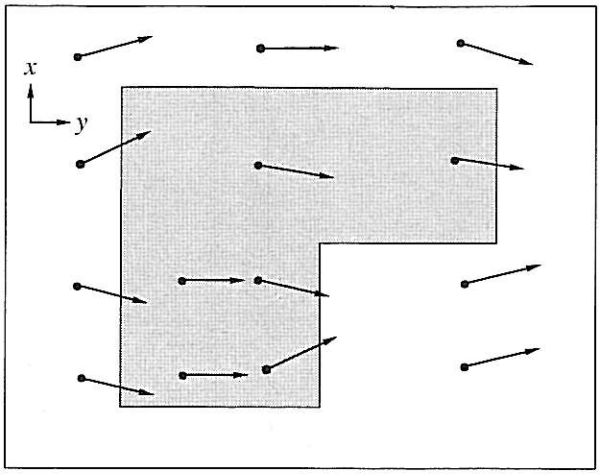

Fig. 8. Bahr electric vectors above the Γ-shaped inclusion.

phase diagrams of the impedance tensor, providing fairly reliable constraints on the deep structure.

It would be of interest to compare the method of polar diagrams with a standard method of the separation of local and regional effects, for example, with the method of Bahr [1988]. We remind the reader that the Bahr method involves the following three limitations: (a) the frequency must be low enough to neglect the local magnetic anomaly and the inductive part of the local electric anomaly produced by a shallow heterogeneity, (b) the regional background must be two-dimensional, and (c) the longitudinal and transverse regional impedances must differ in phase significantly.

The Bahr method is based on relation (17) with a real matrix of local electric distortion [**e**] and a regional 2-D impedance [$\mathbf{Z}^R$]. If the x axis is oriented along a regional strike, we have

$$[\mathbf{Z}] = \begin{bmatrix} Z_{xx} & Z_{xy} \\ Z_{yx} & Z_{yy} \end{bmatrix} = \begin{bmatrix} e_{xx} & e_{xy} \\ e_{yx} & e_{yy} \end{bmatrix} \begin{bmatrix} 0 & Z^{\parallel} \\ -Z^{\perp} & 0 \end{bmatrix} = \begin{bmatrix} -e_{xy}Z^{\perp} & e_{xx}Z^{\parallel} \\ -e_{yy} & e_{yx}Z^{\parallel} \end{bmatrix}, \quad (32)$$

where $Z_{xx} = -e_{xy}Z^{\perp}$, $Z_{yx} = -e_{yy}Z^{\perp}$, and $Z_{xy} = e_{xx}Z^{\parallel}$, $Z_{yy} = e_{yx}Z^{\parallel}$. Here, the columns of the matrix [**Z**] consist of in-phase or antiphase components that satisfy the conditions

$$\begin{aligned} \mathrm{Im}\{Z_{xx}(\alpha)\bar{Z}_{yx}(\alpha)\} &= 0, \\ \mathrm{Im}\{Z_{xy}(\alpha)\bar{Z}_{yy}(\alpha)\} &= 0. \end{aligned} \quad (33)$$

Thus, in order to determine the strike of a regional 2-D structure, we have to find the rotation angle α of the matrix [**Z**] providing the solution to system of equations (33):

$$\alpha = \frac{1}{2}\arctan\frac{\mathrm{Im}(Z_{yx}\bar{Z}_{xx} + Z_{xy}\bar{Z}_{yy})}{\mathrm{Im}(Z_{xx}\bar{Z}_{yy} + Z_{xy}\bar{Z}_{yx})}, \quad (34)$$

where α determines the regional strike azimuth α_R accurate to $\pi/2$. Knowing α_R, phases of the longitudinal and transverse regional impedances can easily be calculated:

$$\begin{aligned} \arg Z^{\parallel} &= \arctan\frac{\mathrm{Im}[Z_{xy}(\alpha_R) + Z_{yy}(\alpha_R)]}{\mathrm{Re}[Z_{xy}(\alpha_R) + Z_{yy}(\alpha_R)]}, \\ \arg Z^{\perp} &= \pi + \arctan\frac{\mathrm{Im}[Z_{xx}(\alpha_R) + Z_{yx}(\alpha_R)]}{\mathrm{Re}[Z_{xx}(\alpha_R) + Z_{yx}(\alpha_R)]}. \end{aligned} \quad (35)$$

Along with regional characteristics, we can obtain certain information on local structures. For example, let an electric field $\mathbf{e}^y$ arise when a local structure is excited by a unit electric field linearly polarized along the y axis, i.e., normal to the strike of the regional structure:

$$\mathbf{e}^y = \begin{bmatrix} e_{xx} & e_{xy} \\ e_{yx} & e_{yy} \end{bmatrix} \begin{bmatrix} 0 \\ 1 \end{bmatrix} = \begin{bmatrix} e_{xy} \\ e_{yy} \end{bmatrix}. \quad (36)$$

Comparing (36) with (32), we find the angle β^y between the y axis and the vector $\mathbf{e}^y$. Measuring β^y clockwise from the y axis, we have

$$\beta^y = -\arctan\frac{e_{xy}}{e_{yy}} = -\arctan\frac{Z_{xx}}{Z_{yx}} \approx -\arctan\mathrm{Re}\frac{Z_{xx}}{Z_{yx}}, \quad (37)$$

where the ratio Z_{xx}/Z_{yx} is approximated by a positive or a negative real value. A map characterizing the direction of the vector $\mathbf{e}^y$ can be used to reveal effects of flowing around and concentration (the current flows around a higher resistivity body and concentrates in a lower resistivity body) and classify a shallow structure with respect to its resistivity.

Now, we return to the model containing a shallow Γ-shaped inclusion and a regional 2-D prism (Fig. 4). Applying the Bahr method to this model at the period $T = 640$ s, we find the strike of the regional prism and the phases of the longitudinal and transverse impedances with an accuracy of no more than 3°. The electric vectors $\mathbf{e}^y$ determined by the Bahr method are mapped in Fig. 8. The flow around the shallow inclusion of a higher resistivity is evident here.

We compare these results with the results obtained by the method of polar diagrams. Phase diagrams of the impedance tensor are inferior to the Bahr method as regards the accuracy of determination of the regional strike and phases of the regional impedance, but diagrams of the E polarized impedance resolve more effectively the shape of a shallow inclusion of a higher resistivity. Thus, the method of polar diagrams and the Bahr method complement each other. The combined application of these two methods is particularly useful because the method of polar diagrams is largely free from the structural and frequency limitations characteristic of

the Bahr method and other standard methods widely applied to the separation of local and regional effects.

The Counil–Le Mouel–Menvielle method underlying the construction of polar diagrams of the H and E polarized impedances is rather rarely applied in the practice of magnetotellurics. We hope that the results obtained in our work with the use of these diagrams will draw the attention of readers to this interesting method.

ACKNOWLEDGMENTS

We are grateful to B.S. Svetov for discussion and constructive criticism. This work was supported by the Russian Foundation for Basic Research, project nos. 04-05-64970 and 05-05-65082.

REFERENCES

1. K. Bahr, "Interpretation of Magnetotelluric Impedance Tensor: Regional, Induction, and Local Telluric Distortion," J. Geophys. **62**, 119–127 (1988).
2. M. N. Berdichevsky, *Electric Survey by the Magnetotelluric Profiling Method* (Nedra, Moscow, 1968) [in Russian].
3. M. N. Berdichevsky and V. I. Dmitriev, "Basic Principles of Interpretation of Magnetotelluric Sounding Curves," in *Geoelectric and Geothermal Studies*, Ed. by A. Adam (Akademiai Kiado, Budapest, 1976).
4. M. N. Berdichevsky, L. L. Vanyan, and Nguen Than Van, "Polar Phase Diagrams of the Magnetotelluric Impedance," Fiz. Zemli, No. 2, 19–23 (1993).
5. M. N. Berdichevsky and V. I. Dmitriev, "Inverse Problems of Magnetotellurics: A Modern Formulation," Fiz. Zemli, No. 4, 12–29 (2004) [Izvestiya, Phys. Solid Earth **40**, 276–292 (2004)].
6. T. G. Caldwell, H. M. Bibby, and Brown, "The Magnetotelluric Phase Tensor," Geophys. J. Int. **158**, 457–469 (2004).
7. J. L. Counil, J. L. Le Mouel, and M. Menvielle, "Associate and Conjugate Directions Concepts in Magnetotellurics," Annales Geophysicae **4** (B2), 115–130 (1986).
8. Nguen Than Van, Candidate's Dissertation in Mathematics and Physics (MGU, Moscow, 1991).
9. E. Yee and K. V. Paulson, "The Canonical Decomposition and Its Relationships to Other Forms of Magnetotelluric Impedance Tensor Analysis," Geophys. J. **61**, 173–189 (1987).